Distinct Stromal Cell Populations Define the B-cell Acute Lymphoblastic Leukemia Microenvironment

Mauricio N. Ferrao Blanco[1], Bexultan Kazybay[1], Mirjam Belderbos[1], Olaf Heidenreich[1], Hermann Josef Vormoor[1,2]

[1] Princess Máxima Center for Pediatric Oncology, Utrecht, the Netherlands
[2] University Medical Center Utrecht, Utrecht, the Netherlands

Abstract

The bone marrow microenvironment is critical for B-cell acute lymphoblastic leukemia (B-ALL) but its cellular heterogeneity remains poorly defined. Here, we employed single-cell RNA sequencing to comprehensively characterize the stromal and hematopoietic niches in pediatric B-ALL. Our analysis revealed two distinct mesenchymal stromal cell (MSC) populations as primary leukemia-supportive niches: early mesenchymal progenitors and adipogenic progenitors. Single-cell transcriptomic analysis infers that ALL blasts use distinct cell-cell interactions to communicate with the different stromal populations. Purified adipogenic progenitors from the bone of children with ALL support survival of the leukemic blasts *ex vivo* and their signature is enriched in relapse samples. Our data establish adipogenic progenitors as a distinct and novel component of the ALL niche.

Introduction

The bone marrow microenvironment is a highly specialized tissue consisting of different cell types and extracellular matrix proteins, essential for regulating hematopoiesis and skeletal regeneration [1]. Central to this intricate network are mesenchymal stromal cells (MSCs), a heterogeneous population encompassing multipotent progenitors of skeletal lineages [2, 3]. These MSCs contribute to the formation of specialized niches within the bone marrow, which provide essential support for hematopoietic stem cell (HSC) function, including homing, quiescence, and lineage commitment [4-6].

The dynamic interplay between leukemic cells and the bone marrow microenvironment is increasingly recognized as a critical factor in hematological malignancies, including B-cell acute lymphoblastic leukemia (B-ALL) [7]. Leukemic cells actively reprogram their microenvironment to create a supportive niche that promotes survival, proliferation, and resistance to therapy [8-10]. While previous studies have implicated a key role of the bone marrow microenvironment in B-ALL, a comprehensive understanding of its cellular heterogeneity remains elusive.

To address this knowledge gap, we conducted a comprehensive single-cell RNA sequencing analysis of the bone marrow microenvironment in pediatric B-ALL. By systematically characterizing the stromal, immune, and leukemic compartments, we identified two distinct MSC populations— early mesenchymal progenitors and adipogenic progenitors—as key contributors to the leukemia-supportive niche. Notably, our findings reveal a previously unrecognized role for adipogenic progenitors in the leukemic niche and shed light on the complexity of the cellular micro-environment in B-ALL.

Results

The single cell bone marrow landscape of B-ALL

To comprehensively characterize the bone marrow microenvironment in B-ALL, we employed flow cytometry to isolate leukemic (CD19+), hematopoietic (CD45+CD235a+), and non-hematopoietic (CD19-CD45-CD235a-) mononuclear cells from patient samples (Figure 1A). The identity of the non-hematopoietic fraction was confirmed by its ability to form colony-forming unit fibroblasts (CFU-Fs), express MSC markers (CD90, CD73, CD105), and differentiate into adipocytes and osteoblasts (Supplementary Figure 1). We generated a single-cell transcriptomic map of the stromal, hematopoietic, and leukemic compartment (figure 1B). After quality control and doublet exclusion, 28,333 high-quality cells were obtained and integrated into a single dataset for further analysis.

Unsupervised clustering identified nine major cell populations based on the expression of lineage-specific markers (Figure 1C; Supplementary Table 2). These clusters corresponded to stromal cells (cluster 8, 2170 cells, expressing *CXCL12*, *THY1* and *FN1*), erythroblasts (cluster 7, 1237 cells, expressing *HBD*, *TFRC* and *GYPA*), CD4 T cells (cluster 2, 2791 cells, expressing

CCR7, *CAMK4* and *CD28*), CD8 T cells (cluster 3, 6049 cells, expressing *CD8A*, *CD8B* and *GZMA*), hematopoietic stem progenitor cells (cluster 6, 814 cells, expressing *MPO, MEIS1, SPINK2* and *AVP*), monocytes (cluster 5, 2156 cells, expressing *S100A8*, *LYZ* and *CD14*), dendritic cells (cluster 4, 265 cells, expressing *IRF7*, *IRF8* and *PLD4*), mature B cells (cluster 1, 740 cells, expressing *CD19*, *CD22* and *MS4A1*) and leukemic cells (cluster 0, 12111 cells, expressing *CD19*, *CD22* and *MME*) (figure 1C). Expression of the hematopoietic marker *PTPRC,* encoding CD45*,* was overall expressed with exception of erythroblasts and stromal cells. Further discrimination between leukemic and mature B cells was based on the aberrant karyotype of ALL cells, inferred by copy number variation analysis (Supplementary Figure 2). Unbiased cell type recognition confirmed the cell annotation and mapped leukemic cells to pro-B cells, confirming their immature phenotype (Supplementary Figure 3A). Gene ontology enrichment analysis validated the cellular identity of each cluster, for example, stromal cells are enriched on genes associated with collagen-containing extracellular matrix while T cells with processes associated with T cell activation (figure 1D).

In summary, the data presented here provide a comprehensive single-cell transcriptomic blueprint of the stromal and hematopoietic bone marrow microenvironment in pediatric B-ALL.

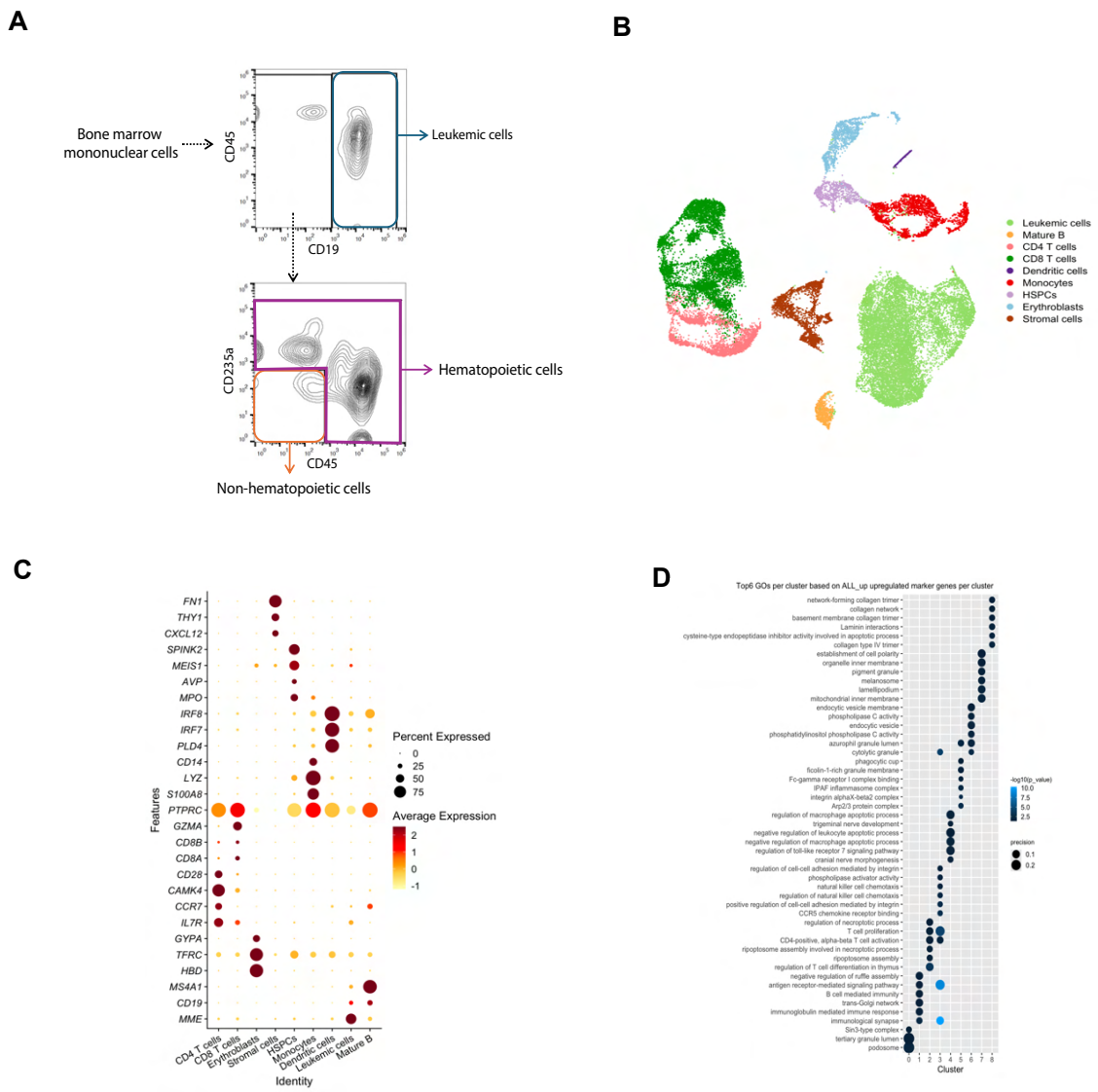

Figure 1. Integrated analysis of the B-ALL bone marrow microenvironment. A) Gating strategy for the enrichment of leukemic cells (CD19+), hematopoietic cells (CD45+CD235a+) and stromal cells (negative for all markers). B) Uniform Manifold Approximation and Projection (UMAP) plot showing cell clusters from the analysis of 28,333 cells integrated from 9 patient

samples. C) DotPlot representation of gene expression of typical cell cluster markers, 3 markers per cluster. D) Enriched gene ontology (GO) terms of differentially expressed genes in the cell clusters, leukemic cells (cluster 0), mature B cells (cluster 1), CD4 T cells (cluster 2), CD8 T cells (cluster 3), dendritic cells (cluster 4), monocytes (cluster 5), HSPCs (cluster 6), erythroblasts (cluster 7), stromal cells (cluster 8).

Identification of distinct stromal cell populations

The stromal landscape in B-ALL remains largely unexplored. In-depth analysis of the stromal cell cluster revealed two distinct populations: early mesenchymal progenitors, expressing stromal markers *THY1*, *MGP*, and *FN1* without lineage markers, and adipogenic progenitors, overexpressing adipogenic markers *LPL*, *PPARG*, and *LEPR* (Figures 2A and 2B). Pseudotime analysis indicated a more primitive state for early mesenchymal progenitors compared to adipogenic progenitors (Figure 2C). To elucidate the transcriptional regulation of stromal cell fate specification, we assessed the activity of key transcription factors using DoRothEA [11]. Adipogenic progenitors exhibited high activity of adipogenic master regulators CEBPA, CEBPB, CEBPG, and PPARG [12], while early mesenchymal progenitors showed elevated FOXP1/2 activity, associated with skeletal stem progenitor cells [13] (figure 2D). Signaling pathway analysis suggest higher MAPK, PI3K and JAK/STAT signaling in adipogenic progenitors compared with early mesenchymal progenitors, consistent with their role in adipogenesis [14-16] (Figure 2E). Gene set enrichment analysis demonstrated that adipogenic progenitors were enriched in extracellular matrix-related genes, characteristic of fate-committed stromal cells (Figure 2F).

By comparing our data with a human bone marrow stromal cell atlas [17], we mapped early mesenchymal progenitors to fibro-MSCs (Figure 2G and Supplementary Figure 3B), an early mesenchymal progenitor population also resembling previously described skeletal stem cells in mice and humans [18]. In contrast, adipogenic progenitors mapped to adipo-MSCs, which resemble reported marrow adipogenic lineage precursors and Adipo-CXCL12-abundant-reticular (Adipo-CAR) cells in mice [19, 20].

Overall, our findings delineate the transcriptomic diversity within the stromal niche in B-ALL, providing novel insights into the cellular heterogeneity of this critical microenvironment.

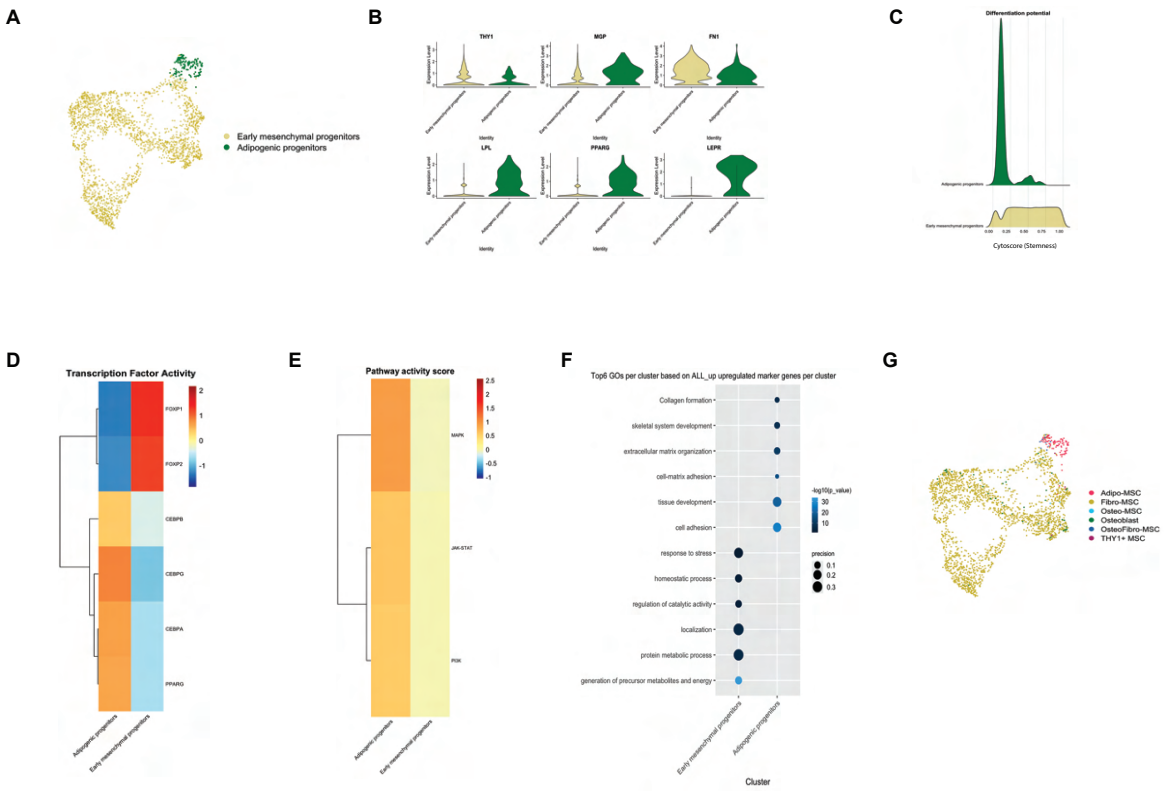

Figure 2. Characterization of the B-ALL stromal niche. A) UMAP representation of the stromal clusters. B) Violin plots representation of gene expression. C) Ridge plot showing the distribution of Cytotrace scores for adipogenic and early mesenchymal progenitors. Each ridge represents a different stromal cell population, with adipogenic progenitors in green and early mesenchymal progenitors in yellow. The x-axis represents the Cytotrace score, which reflects the differentiation trajectory of cells. A higher Cytotrace score indicates a higher stemness profile. The y-axis represents the density of cells at a particular Cytotrace score. Differences in differentiation potential between adipogenic and early mesenchymal progenitors. D) Heatmap representation of transcription factor activity score. E) Heatmap depicting pathway activity analysis. F) Enriched gene ontology (GO) terms of differentially expressed genes in the cell clusters. G) UMAP plot showing the annotation after mapping the stromal cluster to the reported by Bandyopadhyay et al, 2024.

Functional heterogeneity of mesenchymal stromal cell populations

To further characterize these stromal populations, we developed a FACS sorting strategy based on markers identified through our scRNA-seq analysis (Figure 3A & 3B). Adipogenic progenitors were defined by the high expression of *CDH11* (Cadherin 11) and *VCAM1* (CD106), while early mesenchymal progenitors were negative for these markers and positive for CD81 and *THY* (CD90). Notably, commonly used MSC markers exhibited variable expression among stromal subsets (Figure 3A), highlighting the importance of using comprehensive marker panels when studying MSCs.

To validate our sorting strategy, we performed single-cell RNA sequencing on sorted early mesenchymal and adipogenic progenitors, confirming their transcriptomic profiles (Figure 3C). Pseudotime analysis confirmed the more differentiated state of adipogenic progenitors compared to early mesenchymal progenitors (Figure 3D & E). Functional assays revealed a higher CFU-F formation capacity and proliferation rate in early mesenchymal progenitors, consistent with their stem/progenitor-like phenotype (Figure 3F). Conversely, adipogenic progenitors demonstrated enhanced adipogenic differentiation potential (Figures 3G & H). Overall, these findings confirm the functional divergence of early mesenchymal and adipogenic progenitors.

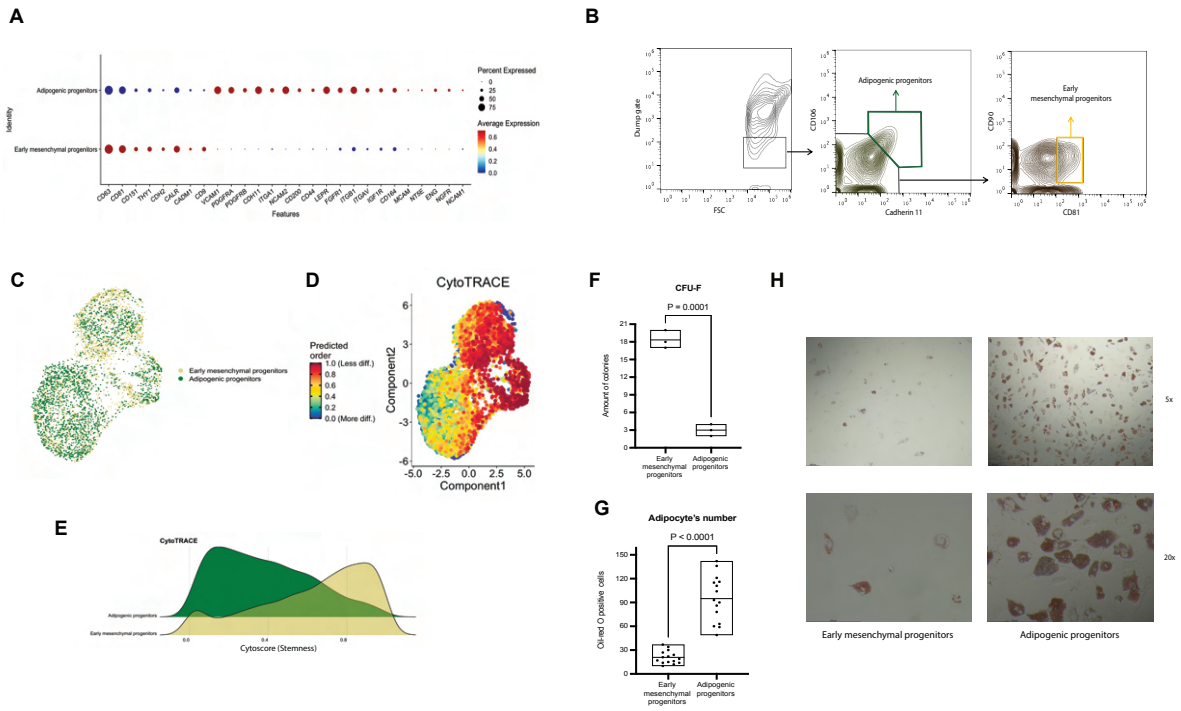

Figure 3. Functional characterization of stromal cell populations in B-ALL. A) Dotplot representation of the gene expression of CD markers in mesenchymal and adipogenic progenitors. B) Gating strategy for the sorting of stromal populations. C) UMAP representation of the two stromal populations analyzed by scRNAseq. D, E) UMAP and ridge plots of the two sorted stromal populations showing the predicted order score in differentiation. F) CFU-F analysis of sorted stromal populations cultured *ex vivo*. The number of colonies per well observed after 10 days were quantified in a 6-well plate (n=3). Two-tailed unpaired t test. G, H) Stromal cells were cultured in adipogenic medium for 14 days. Oil red O stains lipid droplets (red). The number of positive cells were quantified per well in a 96-well plate and normalized to the total cell numbers. Two-tailed unpaired t test.

Early mesenchymal and adipogenic progenitors support leukemogenesis via alternative mechanisms.

Leukemic cell survival is dependent on the microenvironment [21]. To investigate whether stromal heterogeneity influences the production of different supportive factors, we analyzed the expression of known niche factors [21, 22]. RNA expression indicated that different MSC types may produce specific support factors; for example, *SPP1* (osteopontin) and CDH2 (N-Cadherin) was highest in early mesenchymal progenitors, whereas *CXCL12*, *VCAM1* (vascular cell adhesion molecule-1), *ANGPT1* (angiopoietin-1) *IL7* (interleukin 7) and *KITLG* (stem cell factor) was predominantly expressed by adipogenic progenitors (Figure 4A) [23] [24] [25].

To further explore stromal-leukemic cell interactions in an unbiased manner, we performed ligand-receptor interaction analysis (Figure 4B). By quantifying the interactions of the niche cells with the leukemic cells, we found that adipogenic progenitors were categorized as the primary source of ligands interacting with leukemic cells, followed by early mesenchymal progenitors (Figure 4C).

To gain a deeper understanding of the underlaying regulatory mechanisms in the complex communication ecosystem, we further classified the cell-cell interactions into patterns where groups of cells are grouped together if they share a similar communication pattern (Figure 4D). We identified 4 patterns, one related to the hematological module (pattern 1), adipogenic module (pattern 2), erythroid module (pattern 3) and early mesenchymal module (pattern 4). These patterns were characterized by different interactions involving secreted factors, cell-cell contact, and extracellular matrix-receptor signaling (Figure 4E). Interestingly, novel niche-ALL interactions were identified, such as MIF-(CD74 + CXCR4) for early mesenchymal progenitors and MDK-NCL for adipogenic progenitors (Supplementary Figure 4).

To validate these findings, we performed co-culture studies using patient-derived B-ALL cells with the two stromal populations. In line with the computational analysis, we observed that both stromal populations supported *ex vivo* survival of primary ALL cells, with adipogenic progenitors performing slightly better than early mesenchymal progenitors (Figure 4F).

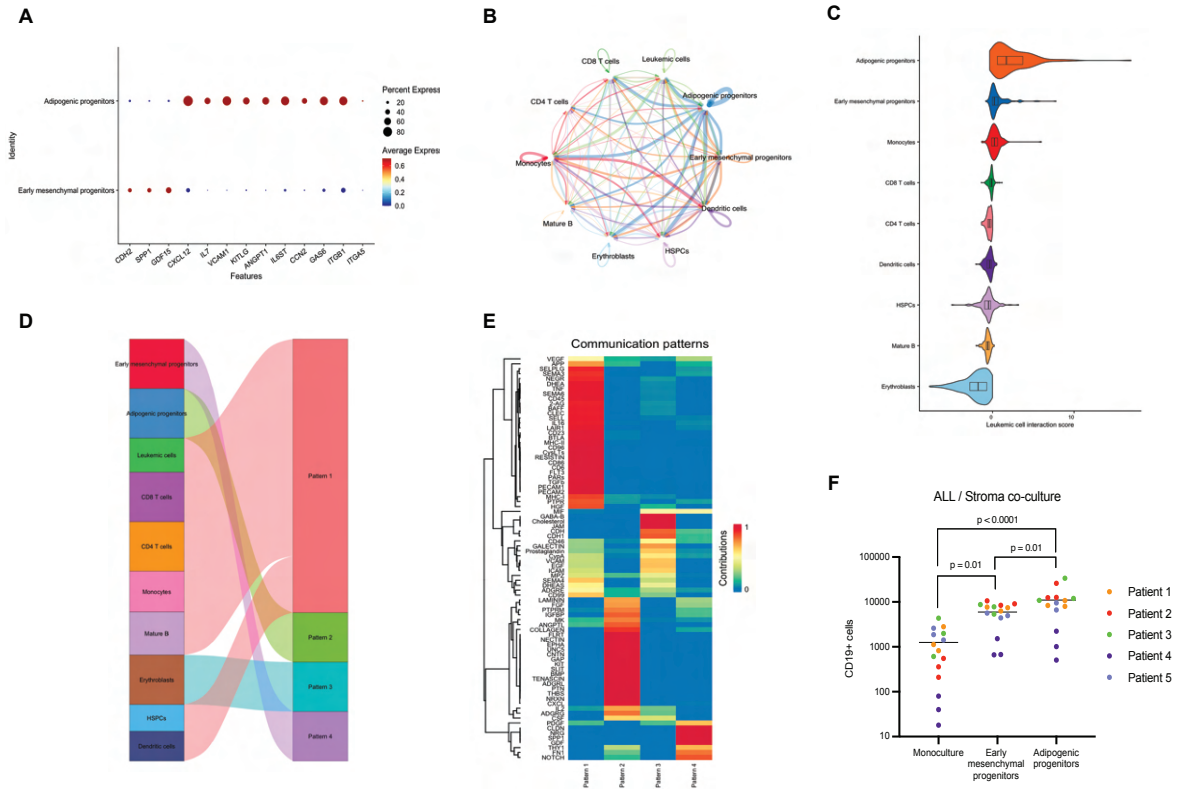

Figure 4. Cell-cell communication analysis in the B-ALL niche. A) Dotplot representation of the gene expression of widely studied niche factors. B) Circle plot showing the interactions between niche cell clusters and leukemic cells. The thickness of the line represents the strength of the interaction. The colors of the lines represent a different cell population. C) Representation of the strength of the cell-cell interaction of the niche cells with the leukemic cells, calculated as a leukemic cell interaction score. D) Non-negative matrix factorization (NMF) to identify modules in the cell-cell interaction pathways between niche cells and leukemic cells. Clusters of cells are grouped into each module. E) Heatmap depicting the cell-cell communication pathways contributing to each pattern identified in D. F) Absolute number of CD19+ leukemic cells per well after seven days of monoculture or co-culture with adipogenic and mesenchymal progenitors. Colors depict different patients. Two-Way ANOVA with Turkey's multiple comparisons test.

Stromal niche composition and clinical implications

The composition of the stromal niche varied between B-ALL patients (Figure 5A). To assess the prevalence of stromal subpopulations in a larger cohort, we performed gene expression deconvolution on RNA-seq data from 265 pediatric B-ALL patients. Adipogenic progenitor gene signatures exhibited a bimodal distribution, suggesting distinct patient clusters (Figure 5 B, C & D). The abundance of adipogenic progenitors did not correlate with leukemic burden (Figure 5E), implying a potential biological role independent of leukemia cell percentage. Importantly, the adipogenic progenitor signature was enriched in patients experiencing relapse, suggesting its involvement in disease progression (Figure 5F).

These findings highlight the heterogeneity of the stromal niche in B-ALL and suggest that adipogenic progenitors may play a crucial role in the leukemic niche.

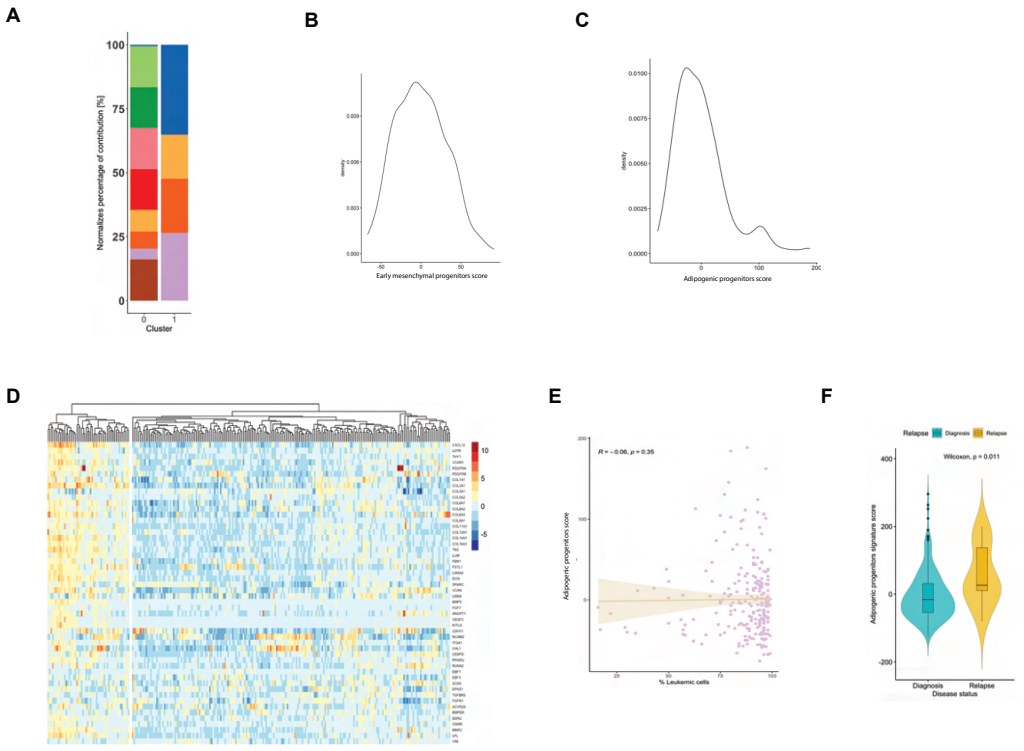

Figure 5. Distinct distribution of stromal cells in B-ALL bone marrow niche. A) Bar plot representing the distribution of stromal cell populations between the different patients analyzed in this study by single-cell RNA sequencing. Mesenchymal progenitors (cluster 0) and adipogenic progenitors (cluster 1). Each patient sample is represented with a color. B) Sample distribution according to the mesenchymal and C) adipogenic progenitor signature. D) Heatmap representation of the adipogenic signature genes (y) across the bulk RNA-seq data of 265 patient samples (x). E) Correlation analysis between adipogenic progenitor signature score and the percentage of leukemic cells in bone marrow samples. F) Analysis of the adipogenic progenitor signature in patents at diagnosis and relapse.

Discussion

The bone marrow microenvironment is a complex and dynamic tissue that plays a critical role in hematopoiesis and leukemogenesis. Our study provides a comprehensive single-cell transcriptional landscape of the B-ALL niche, revealing a previously unappreciated heterogeneity within the stromal compartment. By identifying distinct early mesenchymal and adipogenic progenitor populations, we have unveiled a more nuanced understanding of the cellular composition of the leukemia-supportive niche.

Our findings challenge the traditional view of a homogenous stromal population in B-ALL and highlight the importance of considering cellular heterogeneity in the stromal niche. The functional characterization of early mesenchymal and adipogenic progenitors revealed distinct properties, with early mesenchymal progenitors exhibiting a more stem-like phenotype and adipogenic progenitors demonstrating enhanced differentiation capacity. These results suggest that the bone marrow stroma is composed of a continuum of cell states, with early mesenchymal progenitors representing a more primitive population that gives rise to adipogenic and potentially other stromal cell types. These findings are consistent with previous studies describing the heterogeneity of bone marrow MSCs in normal hematopoiesis [17, 19, 20, 26, 27]. However, our study provides new insights into the specific functional roles of these subpopulations in the context of B-ALL.

The observed difference in proliferation rate between early mesenchymal and adipogenic progenitors suggests that previous studies have overlooked the heterogeneity of the niche due to the selection bias associated with *ex vivo* propagation of MSCs. The more differentiated adipogenic progenitors are less efficient at expanding in culture, leading to an overrepresentation of early mesenchymal progenitors in *ex vivo*-derived stromal populations. This could have contributed to the oversight of the role of adipogenic progenitors in previous studies.

Our study reveals that there are distinct stromal niches with which ALL cells can interact. More importantly, our data suggest that ALL cells utilize different modes of interaction with these diverse niche cells. We have previously demonstrated the involvement of N-Cadherin in

leukemia cell support [8], and now confirm that it is expressed on the early mesenchymal progenitors. In contrast, CXCL12, known to support ALL [25, 28], is primarily expressed by adipogenic progenitors. This complexity underscores the challenges in targeting the niche, as leukemic cells can engage with various environments to survive.

A key finding of our study is the identification of adipogenic progenitors as a major component of the leukemic niche. These cells resemble previously described marrow adipogenic lineage precursors (MALPs) and Adipo-CXCL12-abundant-reticular cells (Adipo-CAR) in mice [19, 20]. Our study provides direct evidence for the involvement of adipogenic progenitor cells in supporting leukemic cell growth and their enrichment at relapse. This observation is in line with previous reports highlighting the role of adipocytes in tumor progression [29]. Adipogenic progenitors exhibited high expression of growth factors, such as IL7 and SCF, and adhesion molecules, such as VCAM1, known to support leukemic cell survival, proliferation and therapy resistance [21, 23, 24]. Interestingly, deletion of IL7 in adipogenic progenitors using the Adipoq-Cre transgene mice resulted in severe impairment of B lymphopoiesis [30], suggesting that B cell development relies on adipogenic progenitors. Additionally, deletion of SCF in adipogenic progenitors diminished HSPCs and myeloid progenitors in the bone marrow and led to the development of macrocytic anemia [31], highlighting the crucial involvement of adipogenic progenitors in steady-state hematopoiesis. These findings highlight the broader role of adipogenic progenitors beyond B-ALL and warrant further investigation in other hematological malignancies, such as acute myeloid leukemia.

The heterogeneity of the stromal niche observed in our patient cohort underscores the complexity of the microenvironment in B-ALL and highlights the need for a comprehensive understanding of the interactions to develop effective niche-targeting therapies. Clustering patient subgroups based on stromal composition may provide additional prognostic information and guide future therapies. Clearly studies with in depth mapping of the leukemic micro-environment in larger patient cohorts are needed to fully comprehend the role of different niche components in leukemic progression and resistance to chemo- and immunotherapy in ALL.

In conclusion, our study provides novel insights into the cellular complexity of the B-ALL microenvironment and identifies adipocyte progenitors as a key novel component of the B-ALL niche.

Limitations of the study

While our study provides valuable insights into the B-ALL microenvironment, it is important to acknowledge certain limitations. First, the focus on pediatric patients may limit the generalizability of our findings to adult B-ALL. Second, the sample size of our single-cell RNA sequencing study may not fully capture the variability within the B-ALL patient population. Third, our analysis was based on gene expression data, and further functional studies are needed to fully elucidate the molecular mechanisms underlying the interactions between stromal cells and leukemic cells.

Materials and methods

Bone marrow samples

Bone marrow aspirates were obtained from pediatric B-ALL patients in conjunction with routine clinical sampling after parents and/or legal guardians had given consent in accordance with institutional review board approval at the Princess Máxima Center. Bone marrow mononuclear cells (BM-MNCs) were isolated from fresh bone marrow aspirates using density gradient centrifugation and cryopreserve for later use. Non-leukemic patient-derived bone marrow mononuclear cells were purchased from Stem Cell technologies (Catalogue 70001). Patient characteristics, including age, gender, genetic risk factors and disease stage can be found in supplementary table 1.

FACs enrichment of stromal, hematopoietic and leukemic cells for scRNAseq

Cryopreserved bone marrow mononuclear cells were thawed and resuspended in RPMI 1640 medium containing 5% FBS and 1 mM EDTA. The cell suspension was passed through a 70 µm mesh and stained for 20 minutes at 4 degrees with an antibody cocktail containing CD19-PE (Catalogue 302207, Clone HIB19, 1:100), CD235a-FITC (Catalogue 349103, Clone HI264, 1:100), CD45-PE-Cy7 (Catalogue 304015, Clone HI30, 1:100), all from Biolegend. Cells were

washed twice with medium followed by 7AAD staining (Catalogue 420404, 1:100) before sorting on a Sony SH800S instrument. Leukemic cells, hematopoietic, and non-hematopoietic cells were sorted in RPMI 1640 medium containing 5% FBS. Samples were kept during the whole procedure at 4 °C. Following enrichment, each of the three cell fractions (leukemic, hematopoietic, non-hematopoietic) were resuspended at a concentration of 1000 cells/µL in PBS + 0.04% BSA. Cells were pooled in a 1:1:1 ratio and the cell suspension was subsequently mixed with a cell suspension from another patient with a different gender (multiplexed boy/girl samples). Subsequently, the cell suspension was loaded into the 10x Genomics Chip as described in 'Single-cell RNA library generation'.

Single-cell RNA-seq library generation

In total, 20,000 cells were loaded for each (multiplexed) sample onto a 10x Genomics Chip G. We used Chromium Next GEM Single Cell 3' GEM, Library & Gel Bead Kit and followed the protocol as provided by 10x Genomics. Sequencing was performed on Illumina NovaSeq 6000 sequencer and parameters were set according to 10x Genomics recommendations.

A healthy donor sample was included in the scRNA-seq analysis. Only the non-hematopoietic compartment from this sample was sorted and sequenced. While the overall amount of stromal cells was higher in the healthy sample, both mesenchymal and adipogenic progenitors were present in both healthy and B-ALL samples, albeit with different proportions (Supplementary Figure 5).

Data processing and filtering

Reads from the sequencing were aligned to the human genome (GRCh38) using Cell Ranger v3.0.2. Samples were demultiplexed using souporcell based on SNP's and patients were identified based on specific sex genes. Further analysis was performed using R v4.0.2 (https://www.r-project.org/) including several packages which are mentioned in the according section. As an initial step, we filtered cells with less than 200 features. Cells with > 10 % of reads mapping to mitochondrial genes were removed. Doublets/multiplets were excluded using the scDblFinder package with standard parameters [32].

Data integration

All patient scRNAseq datasets were merged into one Seurat object after prefiltering (see section: “Data processing and filtering”). Based on this object, the data was normalized (SCT transform from Seurat with default settings), and principal components calculated (RunPCA from Seurat, npcs set to 30). The IntegrateLayers function was run with RPCA integration method and default settings.

Annotation

Cluster annotation for the full integration of all samples was only applied at a low-resolution level to identify major cell types. Cell types were annotated based on information from literature, functional information from gene sets based on the marker genes of a cluster and unbiased cell type recognition using the Human Primary Cell Atlas in SingleR with standard settings [33]. Additionally, single-cell RNA-seq data of stromal cell populations from the manuscript of Bandyopadhyay et al, Cell 2024 [17], was downloaded from NCBI Gene Expression Omnibus (GSE253355) and loaded into Seurat. Cell type inference of our stromal cluster was performed with this dataset as a reference using SingleR with standard settings.

Marker gene identification

Marker genes per cluster were calculated by the Seurat function FindAllMarkers, using the method “Model-based Analysis of Single-cell Transcriptomics” (MAST) and min-pct set to 0.3. Enriched gene sets per set of marker genes were analyzed as described in the GSEA section.

Gene set enrichment analysis (GSEA)

The gprofiler2 package was used to perform GSEA based on marker genes and differentially expressed genes [34]. The gost function was run with default settings. Ribosomal genes were excluded from the gene lists beforehand and only gene lists with more than 5 remaining genes sorted by adjusted p value were tested. Before plotting, the identified gene sets were filtered for terms with less than 1000 genes and only terms from GO, Reactome and KEGG were plotted.

Signal pathway and transcription factor activity

We used the R package PROGENy to estimate signaling pathway activities for each cell and summarized the scores for each cluster [35]. Transcription factor activities were estimated with viper for each cell based on the regulons from DoRothEA [11, 36]. The scores were summarized per cluster and most variable TFs selected for plotting.

Differentiation state prediction

The CytoTRACE algorithm was applied to estimate differentiation hierarchy with default settings [37].

Ligand-receptor interaction analysis

The CellChat algorithm was applied to perform an unbiased ligand-receptor interaction analysis with default settings [38].

Inference of copy number variation.

The SCEVAN package was used to infer CNVs from the scRNA-seq data, using the standard setting [39].

Stromal populations cell sorting

MSC subtypes were isolated from BM-MNCs using fluorescence-activated cell sorting (FACS) based on surface marker expression identified from the single-cell RNA sequencing data. In addition to the analysis of well-known stromal CD markers, we performed an unbiased approach using the sc2marker package with default settings [40].

To exclude hematopoietic and leukemic cells, we used a dump gate strategy at 421 nm emission composed of CD19-BV421 (Catalogue 302233, clone HIB19, 1:100), CD22-BV421 (Catalogue 302523, clone HIB22, 1:100), CD45-BV421 (Catalogue 304031, clone HI30, 1:100), CD235a-BV421 (Catalogue 349131, clone, HI264 1:100). Live/dead exclusion was performed using Zombie green (Catalogue 423111, 1:100). Adipogenic progenitors were sorted as positive for CD106-PE (Catalogue 305805, clone STA, 1:100) and Cadherin 11-APC (Catalogue 368705, clone 16G5, 1:100), while mesenchymal progenitors were negative for these markers and positive for CD81-PE-Cy7 (Catalogue 349511, clone 5A6, 1:100) and CD90-AF700 (Catalogue 328119, clone 5E10, 1:100).

scRNA seq analysis of mesenchymal and adipogenic progenitors

Sorted MSC subtypes were cultured in MSC medium (DMEM-low glucose supplemented with 10% FBS, 1% Primocin solution and 1 ng/mL bFGF) and incubated at 37 °C with 5% CO2. Cells were expanded and scRNAseq analysis was performed at passage three as described in 'Single-cell RNA library generation'.

Colony-forming unit fibroblast (CFU-F) assays

Sorted cells were seeded in 6-well plate (4.5 x 10^3 cells/well) containing culture medium (DMEM-low glucose supplemented with 10% FBS, 1% Penicillin/Streptomycin solution and 1 ng/mL bFGF) and incubated at 37 °C with 5% CO2. Medium was changed every 3–4 days. At day 10, cells were fixed and stained with 0,5% crystal violet staining solution in methanol. Adherent colonies with more than 50 cells were quantified.

Multipotency assays

Adipogenic and osteogenic differentiation assays was performed in cells at passage three. Adipogenic differentiation was performed in DMEM (Gibco, Catalogue 21885) supplemented with 10% FBS, 1% Penicillin/Streptomycin, 0.5 µM isobutylmethylxanthine (Sigma, I5879), 60 µM indomethacin (Sigma, 17378), 5 µg/mL insulin (Sigma, I9278) and 1 µM dexamethasone (Sigma, D2915) for 2 weeks (medium was changed every 3 days), and quantified by oil red O staining (Sigma, 00625). Osteogenic differentiation was performed in osteogenic medium for 2 weeks (medium was changed every 3 days) and quantified by alizarin red S staining (Sigma, A5533). The osteogenic differentiation medium contained DMEM supplemented with 10% FBS, 1% Penicillin/Streptomycin, 1% glutamine, 50 µg/mL L-ascorbate acid (Sigma, A8960), 10 mM β-glycerophosphate (Sigma, G6376) and 100 nM dexamethasone.

Co-Culture Experiments

Leukemic cells and MSC subtypes were co-cultured in SFEM medium containing antibiotics and incubated at 37 °C with 5% CO2. After 7 days, all cells per well were harvested by aspirating the supernatant as well as trypsinization of attached cells. Both cell suspensions were combined, per well. After washing the cells with PBS, FBS 5%, cells were stained with

CD19-BV421 (Catalogue 302233, clone HIB19, 1:100) and Zombie NIR (1:200, Catalogue 423106) for live/dead exclusion.
Cell viability was assessed using a flow cytometry Cytoflex S, recording all events with a fixed volume of 80 microliters per well.

Gene Set Signature Analysis in Bulk RNA-seq Data

Bulk RNA-seq data generated for routine diagnostics were obtained from the Princess Máxima Center Biobank. A cohort of 265 B-ALL bone marrow patient samples was utilized. The signature of each stromal population was calculated as in the section "Marker gene identification". Each signature was applied to the normalized count data of the bulk-RNAseq data and an average expression value of the genes was calculated per sample to calculate the score.

Statistical Analysis

Unless otherwise stated, statistical significance was assessed by a two-tailed Student's t test or one-way ANOVA with Tukey's or Dunnett's multiple comparison with a p value < 0.05 being considered statistically significant. Statistical analyses were performed using GraphPad Prism 9.0.1. GSEA is performed with the hypergeometric test for overrepresentation (one-sided), followed by multiple comparison correction. The individual method of correction for gProlifer2 is described in the corresponding publications.

Acknowledgements

We would like to thank the single cell sequencing facility, the flow cytometry facility at the Princess Máxima Center, Polina Derevianko, Anita van Oort and Elizabeth Schweighart for their assistance.

Funding

This work has been supported by Horizon Europe's Marie Sklodowska – Curie Actions co-fund project number 101081481 (Butterfly), KiKa project number 329, ERC (grant no. 101114895) and Landsteiner Foundation for Blood Research (grant no. 2305F).

References

1. Ding, L. and S.J. Morrison, *Haematopoietic stem cells and early lymphoid progenitors occupy distinct bone marrow niches.* Nature, 2013. **495**(7440): p. 231-5.
2. Mendez-Ferrer, S., et al., *Mesenchymal and haematopoietic stem cells form a unique bone marrow niche.* Nature, 2010. **466**(7308): p. 829-34.
3. Bianco, P. and P.G. Robey, *Skeletal stem cells.* Development, 2015. **142**(6): p. 1023-7.
4. Kunisaki, Y., et al., *Arteriolar niches maintain haematopoietic stem cell quiescence.* Nature, 2013. **502**(7473): p. 637-43.
5. Greenbaum, A., et al., *CXCL12 in early mesenchymal progenitors is required for haematopoietic stem-cell maintenance.* Nature, 2013. **495**(7440): p. 227-30.
6. Sugiyama, T., et al., *Maintenance of the hematopoietic stem cell pool by CXCL12-CXCR4 chemokine signaling in bone marrow stromal cell niches.* Immunity, 2006. **25**(6): p. 977-88.
7. Duan, C.W., et al., *Leukemia propagating cells rebuild an evolving niche in response to therapy.* Cancer Cell, 2014. **25**(6): p. 778-93.
8. Pal, D., et al., *hiPSC-derived bone marrow milieu identifies a clinically actionable driver of niche-mediated treatment resistance in leukemia.* Cell Rep Med, 2022. **3**(8): p. 100717.
9. Park, C.S., et al., *Stromal-induced epithelial-mesenchymal transition induces targetable drug resistance in acute lymphoblastic leukemia.* Cell Rep, 2023. **42**(7): p. 112804.
10. Witkowski, M.T., et al., *Extensive Remodeling of the Immune Microenvironment in B Cell Acute Lymphoblastic Leukemia.* Cancer Cell, 2020. **37**(6): p. 867-882 e12.
11. Garcia-Alonso, L., et al., *Benchmark and integration of resources for the estimation of human transcription factor activities.* Genome Res, 2019. **29**(8): p. 1363-1375.
12. Wu, Z., N.L. Bucher, and S.R. Farmer, *Induction of peroxisome proliferator-activated receptor gamma during the conversion of 3T3 fibroblasts into adipocytes is mediated by C/EBPbeta, C/EBPdelta, and glucocorticoids.* Mol Cell Biol, 1996. **16**(8): p. 4128-36.
13. He, J., et al., *Dissecting human embryonic skeletal stem cell ontogeny by single-cell transcriptomic and functional analyses.* Cell Res, 2021. **31**(7): p. 742-757.
14. Aouadi, M., et al., *p38MAP Kinase activity is required for human primary adipocyte differentiation.* FEBS Lett, 2007. **581**(29): p. 5591-6.
15. Bost, F., et al., *The extracellular signal-regulated kinase isoform ERK1 is specifically required for in vitro and in vivo adipogenesis.* Diabetes, 2005. **54**(2): p. 402-11.
16. Richard, A.J. and J.M. Stephens, *The role of JAK-STAT signaling in adipose tissue function.* Biochim Biophys Acta, 2014. **1842**(3): p. 431-9.
17. Bandyopadhyay, S., et al., *Mapping the cellular biogeography of human bone marrow niches using single-cell transcriptomics and proteomic imaging.* Cell, 2024. **187**(12): p. 3120-3140 e29.
18. Chan, C.K.F., et al., *Identification of the Human Skeletal Stem Cell.* Cell, 2018. **175**(1): p. 43-56 e21.
19. Zhong, L., et al., *Single cell transcriptomics identifies a unique adipose lineage cell population that regulates bone marrow environment.* Elife, 2020. **9**.

20. Tikhonova, A.N., et al., *The bone marrow microenvironment at single-cell resolution.* Nature, 2019. **569**(7755): p. 222-228.
21. Mendez-Ferrer, S., et al., *Bone marrow niches in haematological malignancies.* Nat Rev Cancer, 2020. **20**(5): p. 285-298.
22. Hughes, A.M., et al., *The Bone Marrow Microenvironment in B-Cell Development and Malignancy.* Cancers (Basel), 2022. **14**(9).
23. Pinho, S., et al., *PDGFRalpha and CD51 mark human nestin+ sphere-forming mesenchymal stem cells capable of hematopoietic progenitor cell expansion.* J Exp Med, 2013. **210**(7): p. 1351-67.
24. Omatsu, Y., et al., *The essential functions of adipo-osteogenic progenitors as the hematopoietic stem and progenitor cell niche.* Immunity, 2010. **33**(3): p. 387-99.
25. Agarwal, P., et al., *Mesenchymal Niche-Specific Expression of Cxcl12 Controls Quiescence of Treatment-Resistant Leukemia Stem Cells.* Cell Stem Cell, 2019. **24**(5): p. 769-784 e6.
26. Baccin, C., et al., *Combined single-cell and spatial transcriptomics reveal the molecular, cellular and spatial bone marrow niche organization.* Nat Cell Biol, 2020. **22**(1): p. 38-48.
27. Wolock, S.L., et al., *Mapping Distinct Bone Marrow Niche Populations and Their Differentiation Paths.* Cell Rep, 2019. **28**(2): p. 302-311 e5.
28. Spiegel, A., et al., *Unique SDF-1-induced activation of human precursor-B ALL cells as a result of altered CXCR4 expression and signaling.* Blood, 2004. **103**(8): p. 2900-7.
29. Shafat, M.S., et al., *Leukemic blasts program bone marrow adipocytes to generate a protumoral microenvironment.* Blood, 2017. **129**(10): p. 1320-1332.
30. Mukohira, H., et al., *Mesenchymal stromal cells in bone marrow express adiponectin and are efficiently targeted by an adiponectin promoter-driven Cre transgene.* Int Immunol, 2019. **31**(11): p. 729-742.
31. Zhang, Z., et al., *Bone marrow adipose tissue-derived stem cell factor mediates metabolic regulation of hematopoiesis.* Haematologica, 2019. **104**(9): p. 1731-1743.
32. Germain, P.L., et al., *Doublet identification in single-cell sequencing data using scDblFinder.* F1000Res, 2021. **10**: p. 979.
33. Aran, D., et al., *Reference-based analysis of lung single-cell sequencing reveals a transitional profibrotic macrophage.* Nat Immunol, 2019. **20**(2): p. 163-172.
34. Kolberg, L., et al., *gprofiler2 -- an R package for gene list functional enrichment analysis and namespace conversion toolset g:Profiler.* F1000Res, 2020. **9**.
35. Schubert, M., et al., *Perturbation-response genes reveal signaling footprints in cancer gene expression.* Nat Commun, 2018. **9**(1): p. 20.
36. Alvarez, M.J., et al., *Functional characterization of somatic mutations in cancer using network-based inference of protein activity.* Nat Genet, 2016. **48**(8): p. 838-47.
37. Gulati, G.S., et al., *Single-cell transcriptional diversity is a hallmark of developmental potential.* Science, 2020. **367**(6476): p. 405-411.
38. Jin, S., et al., *Inference and analysis of cell-cell communication using CellChat.* Nat Commun, 2021. **12**(1): p. 1088.
39. De Falco, A., et al., *A variational algorithm to detect the clonal copy number substructure of tumors from scRNA-seq data.* Nat Commun, 2023. **14**(1): p. 1074.
40. Li, R., et al., *Detection of cell markers from single cell RNA-seq with sc2marker.* BMC Bioinformatics, 2022. **23**(1): p. 276.